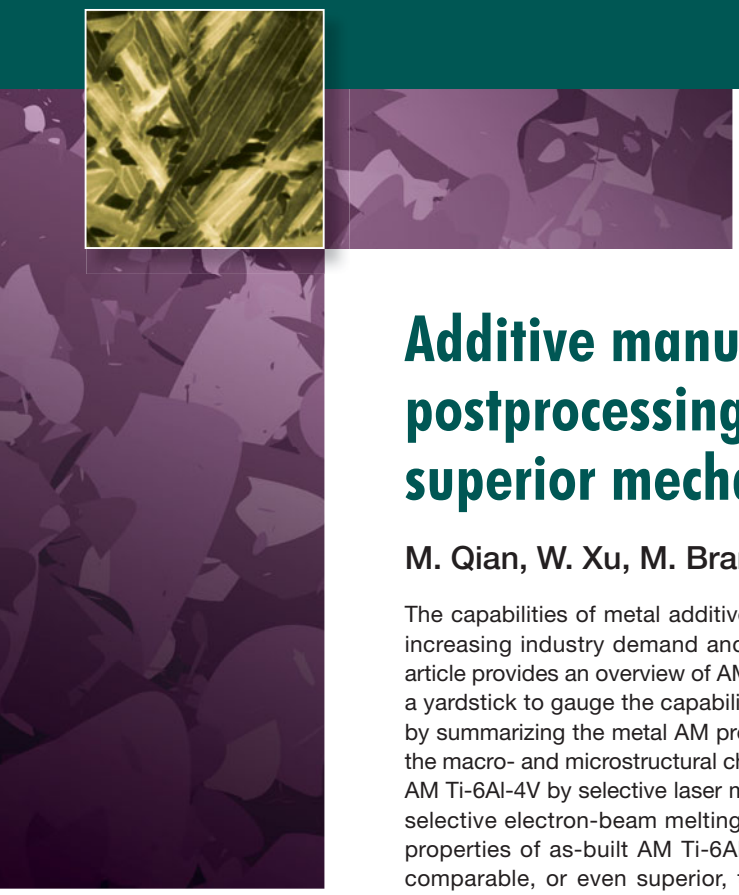

Additive manufacturing and postprocessing of Ti-6Al-4V for superior mechanical properties

M. Qian, W. Xu, M. Brandt, and H.P. Tang

The capabilities of metal additive manufacturing (AM) are evolving rapidly thanks to both increasing industry demand and improved scientific understanding of the process. This article provides an overview of AM of the Ti-6Al-4V alloy, which has essentially been used as a yardstick to gauge the capability of each metal AM process developed to date. It begins by summarizing the metal AM processes existing today. This is followed by a discussion of the macro- and microstructural characteristics, defects, and tensile and fatigue properties of AM Ti-6Al-4V by selective laser melting, laser metal deposition (both powder and wire), and selective electron-beam melting compared to non-AM Ti-6Al-4V. The tensile and fatigue properties of as-built AM Ti-6Al-4V (with machined or polished surfaces) can be made comparable, or even superior, to those of Ti-6Al-4V in the most commonly used mill-annealed condition. However, these properties can exhibit a large degree of scatter and are often anisotropic, affected by AM build orientations. Post-AM surface treatments or both the post-AM surface and heat treatments are necessary to ensure the minimum required properties and performance consistency. Future directions to further unlock the potential of AM of Ti-6Al-4V for superior and consistent mechanical properties are also discussed.

Introduction

Metal additive manufacturing (AM) is no longer solely a prototyping technology; it is now being used for production of industrial parts ranging from orthopedic implants to aircraft components.[1] The last two decades have seen the development of a diversity of metal AM processes. **Figure 1** summarizes these processes categorized in terms of energy source, feedstock form, and additive method with corresponding key equipment manufacturers. In principle, all weldable metals can be fusion-printed today. In a broader sense, all powdered metals can be printed at room temperature using the ExOne binder jetting process (see Figure 1)[2] to achieve a preliminary shape, with the final shape and required properties developed through a subsequent infiltration or sintering process.

Titanium alloys are advanced structural materials that possess an array of unique properties. These include corrosion immunity to seawater, high strength-to-weight ratios, excellent fracture toughness, high-fatigue performance, significant compatibility with composites, long durability with little or no maintenance, and superb biocompatibility. However, titanium-based materials are not easy to machine due to their low thermal conductivity and acute reactivity.[3] In addition, they are difficult to cast since molten titanium is extremely reactive, which is problematic for both melt handling and casting.[3] As a result, historically, titanium components have been mostly machined from forged titanium blanks at a slow speed, entailing prolonged manufacturing cycles and up to 95% of the raw material being lost as scrap (recycling titanium chips from machining is not straightforward).[4,5] The concept of metal AM was therefore especially attractive for the manufacture of titanium components.

From a research perspective, Ti-6Al-4V, which accounts for more than 50% of total titanium usage,[6] has been the single most extensively studied alloy for AM. Apart from the liquid metal printing process, Ti-6Al-4V has been additively manufactured using every other AM process (shown in Figure 1) to gauge the capability of each process.

This article offers an overview of AM and postprocessing of AM Ti-6Al-4V by focusing on microstructures and mechanical properties. The discussion is limited to selective laser melting (SLM), selective electron-beam melting (SEBM), and laser metal (powder and wire) deposition (LMD).

M. Qian, Centre for Additive Manufacturing, School of Engineering, RMIT University, Australia; ma.qian@rmit.edu.au
W. Xu, Department of Engineering, Macquarie University, Australia; wei.xu@mq.edu.au
M. Brandt, Centre for Additive Manufacturing, School of Engineering, RMIT University, Australia; milan.brandt@rmit.edu.au
H.P. Tang, State Key Laboratory of Porous Metal Materials, Northwest Institute for Non-ferrous Metal Research, China; hptang@c-nin.com
doi:10.1557/mrs.2016.215

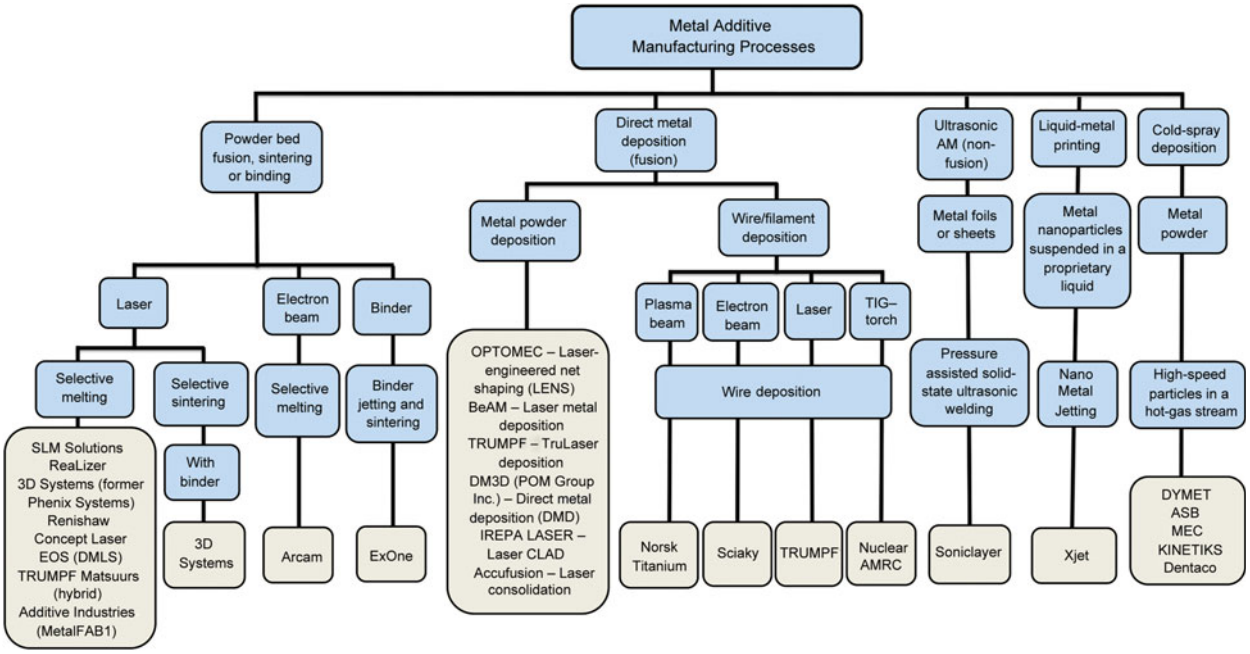

Figure 1. A schematic summary of current metal additive manufacturing (AM) processes.[2]

Macro- and microstructural characteristics of AM Ti-6Al-4V

The manufacturing of each layer of a Ti-6Al-4V component by SLM, SEBM, and LMD involves small-volume melting of the feedstock material (powder or wire), near rapid solidification, and thermal influence from the subsequently built layers (excluding the last few layers).

Melting is the first major phase-transformation process involved. The liquidus temperature (T_l) of Ti-6Al-4V is ~1650 ± 15°C and its solidus temperature (T_s) is ~1605 ± 10°C.[7] It should be noted that compositions of Al and V in Ti-6Al-4V are allowed to vary from 5.5–6.75 and 3.5–4.5, respectively. These variations lead to different liquidus, solidus, and density (4.42–4.43 g cm^{-3}) values. The maximum metal pool temperature during AM of Ti-6Al-4V by laser powder deposition falls in the range of ~2000–2500°C at a laser power of 350 W, deposition rate of 0.13 g/s, and layer thickness of 508 μm.[8] For comparison, a peak melt temperature of 2026°C was measured for laser powder deposition of H13 tool steel under similar AM conditions.[9] This high melt pool temperature can lead to a loss of both Al and V by volatilization.[10]

The increase in oxygen in as-built Ti-6Al-4V by laser AM under argon was found to be less than 300 ppm compared to the feedstock oxygen level.[11,12] For AM of Ti-6Al-4V by SEBM, the oxygen content of the Ti-6Al-4V powder increased progressively from 0.08% (virgin) to 0.19% after being reused 21 times.[10] The critical level of oxygen for press-and-sinter Ti-6Al-4V is about 0.32%, beyond which tensile ductility drops dramatically due to several oxygen-induced microstructural changes.[13]

The maximum cooling rate in the melt pool of Ti-6Al-4V varies in the approximate range of (1.2–4.0) × 10^4°C/s for laser powder deposition[8] (which is ~1.83 × 10^4°C/s for laser powder deposition of H13 steel under similar AM conditions).[9] Molten Ti-6Al-4V solidifies as columnar prior-β grains in all fusion-based metal AM processes reported in literature. The subsequent cooling process is affected by both the number of layers and geometry of the part, and determines the pathways to microstructural development from sub-solidus temperatures to room temperature. Specifically, the pathways are dictated by (1) the initial cooling rate in the as-solidified alloy and (2) the continuously changing thermal gradient in the region of interest during the subsequent AM process.

The initial cooling rates in as-deposited Ti-6Al-4V near the melt pool during laser powder deposition[8] were found to be markedly higher than the critical cooling rates (>18–23°C[14,15] or >420°C[16]) required for martensitic transformation in Ti-6Al-4V. Martensite (α′) is thus commonly observed in AM Ti-6Al-4V by SLM, SEBM, and LMD. However, it can decompose into fully lamellar α/β structures during AM.[17,18] Columnar prior-β grains, which are parallel to the AM build direction and show a $\langle 001 \rangle_\beta$ orientation, are predominant in each AM process. The ⟨001⟩ direction is known to be the favored growth direction of the parent β phase during solidification, which tends to be aligned with the direction of the maximum thermal gradient (i.e., the AM build direction).[19] Much effort has been expended to enable a successful columnar-to-equiaxed transition (CET). However, the large thermal gradient in the AM melt pool prevents the CET from developing in most cases. It was not until recently that researchers reported the CET in laser powder deposition of Ti-6Al-4V at

https://doi.org/10.1557/mrs.2016.215 Published online by Cambridge University Press

a laser power of 1 kW,[8] informed by the CET map proposed by Kobryn and Semiatin[20] for AM of Ti-6Al-4V. The use of high-power laser systems (e.g., 8 kW CO_2 laser) makes it easier to realize CET due to the reduced thermal gradient in the melt pool.[21] Other approaches are being developed to enable the achievement of fine equiaxed grains in AM Ti-6Al-4V. For example, applying deformation to each layer of wire-deposited Ti-6Al-4V has proved to be effective due to subsequent recrystallization.[22]

SLM, SEBM, and LMD can result in similar or distinct microstructures depending on processing and feedstock conditions. **Figure 2** shows some of the microstructural features observed, including martensite (α′), massive α phase (α_m), lamellar α/β, and non-lamellar α and β.[11,12,17,23,24] Literature data on the critical cooling rates for $\beta \rightarrow \alpha'$, $\beta \rightarrow \alpha_m$ and $\beta \rightarrow \alpha$ transformations differ widely.[14–16] These discrepancies can be partially attributed to the different compositions of Ti-6Al-4V used.[5]

The borderline cooling rate for the diffusion-controlled $\beta \rightarrow \alpha$ transformation is below about 20°C/s.[14–16] Above 20°C/s, either the composition-invariant $\beta \rightarrow \alpha_m$ massive transformation occurs, where diffusional activity occurs mainly at the advancing interfaces,[25] or the composition-invariant diffusionless $\beta \rightarrow \alpha'$ martensitic transformation occurs. The $\beta \rightarrow \alpha_m$ transformation has been identified to occur in SEBM Ti-6Al-4V,[24] which contributes to development of SEBM Ti-6Al-4V microstructures. It should be noted that although the columnar prior-β grains show a strong $\langle 001 \rangle_\beta$ orientation or texture parallel to the AM build direction, the α phase that forms during subsequent cooling shows no clear texture or just a random texture.[26]

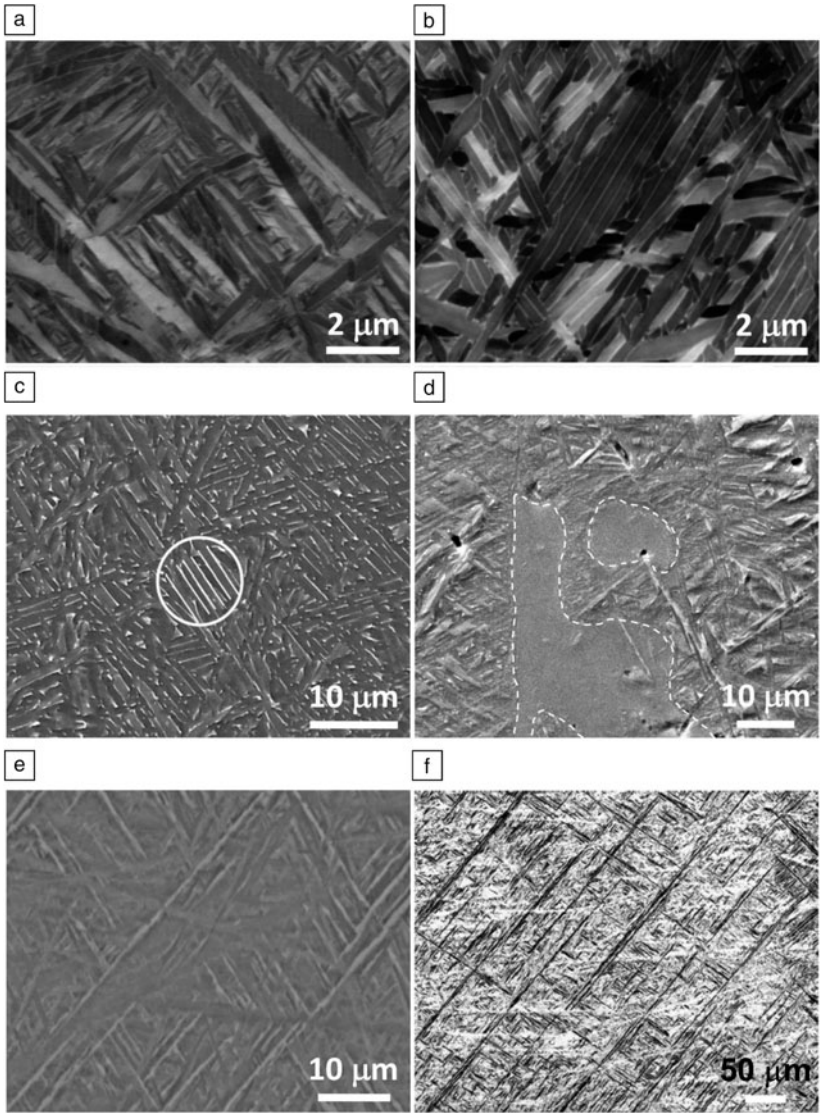

Figure 2. Microstructures of Ti-6Al-4V additively manufactured by selective laser melting (SLM), selective electron-beam melting (SEBM), and laser metal deposition. (a) Fully martensitic (α′) (SLM).[17] (b) Fully lamellar α/β (SLM).[17] (c) Lamellar α/β (circled area), α′ and nonlamellar α and β (SEBM),[23] (d) α′ + massive α grains (α_m) (marked areas) + lamellar α/β (SEBM).[24] (e) α′+ partially decomposed α′ (laser powder deposition). Adapted with permission from Reference 11. © 2015 Elsevier. (f) α′ + partially decomposed α′ (laser wire deposition). Adapted with permission from Reference 12. © 2011 Elsevier.

Defects in AM Ti-6Al-4V

The most common defects observed in AM Ti-6Al-4V are gas-entrapped pores (**Figure 3**a)[23] and lack-of-fusion imperfections (Figure 3b),[23] including unmelted or incompletely melted Ti-6Al-4V particles (Figure 3c).[27] The lack-of-fusion voids are also referred to as lack-of-fusion pores by some researchers. They are mostly irregular in shape and larger than gas-entrapped spherical pores. As such, they can be much more damaging than gas-entrapped spherical pores,[28] especially when their orientations are perpendicular to the tensile loading direction.

In general, the overall porosity or defects in AM Ti-6Al-4V can be controlled to be less than 0.3 vol%,[29–32] but current requirements demand ensuring this to be less than 0.1 vol% at present. A variety of factors can affect the formation of defects. In addition to the AM routes (e.g., scanning patterns) and parameters, the occurrence of gas-entrapped pores seems to be closely related to the feedstock quality. Svensson and Ackelid[30] reported that the use of gas-atomized (GA) Ti-6Al-4V powder containing 0.27 vol% porosity resulted in 0.19 vol% final porosity in SEBM Ti-6Al-4V samples, while the use of lower-porosity (0.17 vol%) GA powder led to lower final porosity (0.11 vol%). GA Ti-6Al-4V powder can contain noticeable internal porosity, as shown in Figure 3d,[28] in which eight out of the 427 GA Ti-6Al-4V particles (1.87%) show gas-entrapped pores.

https://doi.org/10.1557/mrs.2016.215 Published online by Cambridge University Press

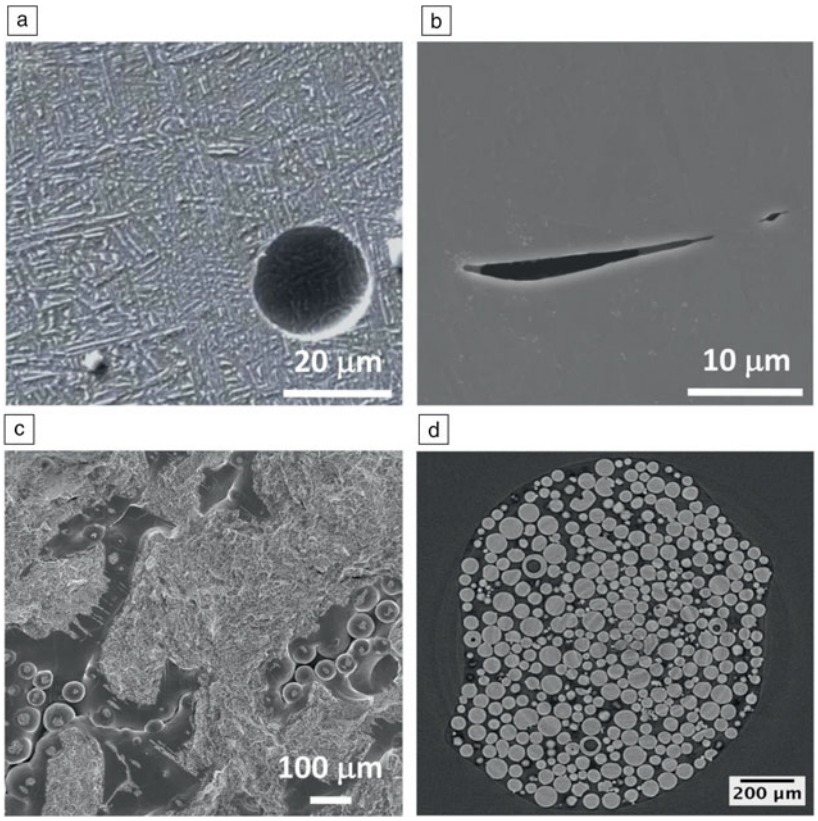

Figure 3. Examples of a gas pore (a) and a lack-of-fusion defect in selective electron-beam melting (SEBM)-fabricated (b) Ti-6Al-4V.[23] (c) Unmelted and incompletely melted Ti-6Al-4V particles observed on an SEBM Ti-6Al-4V tensile fracture surface. Adapted with permission from Reference 27. © 2016 Elsevier. (d) Synchrotron x-ray microtomograph of internal porosity in Arcam gas-atomized (GA) Ti-6Al-4V particles. Eight out of the 427 GA Ti-6Al-4V particles or 1.87% of the particles examined show internal porosity. Adapted with permission from Reference 28. © 2016 Springer.

Ti-6Al-4V powder produced by the plasma-rotating electrode process (PREP) is known to contain much less porosity (0.017 vol%)[18] than GA Ti-6Al-4V powder. The use of PREP powder is therefore expected to favor lower final porosity. However, it is challenging to produce fine PREP Ti-6Al-4V powder (≤45 μm) due to both the low density of molten Ti-6Al-4V (4.12 g cm^{-3} at 1700°C)[33] and the maximum rotation speed that can be realized (≤18,000 rpm).

Other factors that may contribute to the final porosity include evaporation of the low-melting-point Al due to the high-temperature melt pool (2000–2500°C), which may lead to Al vapor-entrapped pores, and the reduced solubility of gas in the melt pool from 2500°C to 1650°C (liquidus). Modeling and simulations have shown that dynamic flow patterns in the melt pool (caused by a variety of factors) can also affect the porosity formation process.[34]

It is important to note that even though the porosity in AM Ti-6Al-4V can be controlled to be as low as 0.1 vol%, the number of damaging pores can still be significant. To illustrate this, consider a 10-mm diameter and 100-mm long AM Ti-6Al-4V rod containing 0.1 vol% porosity. Assume that all of the pores are spherical and each pore is 30 μm in diameter, which is large enough to be damaging for high-cycle fatigue (HCF) performance.[35] The presence of 0.1 vol% porosity means that, on average, there exist 5555 pores in each millimeter-thick slice of the rod for a spatially uniform pore distribution. Nonuniform pore distributions can be more damaging. The lack-of-fusion defects and large gas-entrapped pores are thus of real concern in fatigue critical components.

Tensile properties of AM Ti-6Al-4V

Ti-6Al-4V is most commonly used in the mill-annealed condition. However, Ti-6Al-4V can be hardened in sections up to 25.4 mm thickness via a solution treatment and aging (STA) process.[36] **Table I** lists the minimum tensile properties of mill-annealed and STA Ti-6Al-4V at room temperature as a point of reference for the discussion of the tensile properties of AM Ti-6Al-4V.

Laser AM Ti-6Al-4V and effects of heat treatment

The following discussion is based on two recent reviews of the mechanical properties of laser AM Ti-6Al-4V.[37,38] **Figure 4** summarizes the tensile properties of AM Ti-6Al-4V available from literature,[39–43] with Figure 4a focusing on laser AM and Figure 4b on SEBM in both the as-built and heat-treated conditions. The heat treatments involved cover commonly used sub-transus (i.e., below ~996°C in the α-β region) and super-transus (i.e., above ~996°C in the β region) heat-treating processes for Ti-6Al-4V, as well as hot isostatic pressing (HIP), which simultaneously applies high gas pressure (usually with argon) to reduce porosity and heal microcracks. The β transus of Ti-6Al-4V varies in the range 996 ± 14°C, depending on the actual Al (5.5–7.5) and V (3.5–4.5) contents.

The following observations are notable comparing Figure 4a with Table I and other literature data on laser AM Ti-6Al-4V.[37–47]

- The tensile ductility of laser AM Ti-6Al-4V in the as-built condition, either by powder bed fusion or direct deposition, is often below the minimum requirement (10%) for mill-annealed Ti-6Al-4V, while the tensile strengths can easily meet the requirement.
- Applying sub-transus heat treatments above the effective martensite decomposition temperature (780°C)[44] to SLM Ti-6Al-4V can increase tensile ductility, but to achieve greater than 10% tensile elongation, it is generally necessary to anneal the SLM Ti-6Al-4V at temperatures ≥940°C, followed by either furnace cooling or air cooling.[45,46]

https://doi.org/10.1557/mrs.2016.215 Published online by Cambridge University Press

Table I. Minimum tensile properties of mill-annealed and solution-treated and aged (STA) Ti-6Al-4V at room temperature (YS, yield strength; UTS, ultimate tensile strength).

Bars and Billets (mm)	Condition	UTS (MPa)	0.2% YS (MPa)	Elongation (%)	Reduction in area (%)	Specification
For all sizes in general	Annealed	895	828	10	25	ASTM B348
<12.7	STA	1137	1068	10	20	Mil-T-9047G
12.7–25.4	STA	1103	1034	10	20	Mil-T-9047G
Microstructure	Mill-annealed: equiaxed α grains (cross-sectional view is often elongated) plus ~10 vol% grain boundary (GB) β					
	STA: bimodal; ~30–40 vol% equiaxed α grains (cross-sectional view is often elongated) plus a fine lamellar α/β matrix from decomposed α′					

Water quenching is not favored, as the resulting martensite (α′) structure is much coarser (~1–2-μm-thick α′ laths) than the initial SLM α′ structure (300–500-nm-thick α′ laths).[47] Post-AM heat treatments below 780°C generally fail to show any noticeable influence on the tensile properties of AM Ti-6Al-4V.[32,34,43]

- Super-transus heat treatments can increase the tensile elongation to above 10% under air or furnace cooling conditions, with or without subsequent stabilization annealing.[37] In addition, it can transform the columnar prior-β grains into equiaxed β grains through a proposed shearing mechanism, which appears to occur only at high cooling rates.[47] However, the actual contribution of this solid-state columnar-to-equiaxed transition to mechanical properties remains unclear, because noticeable grain coarsening occurs at super-transus temperatures.
- AM Ti-6Al-4V exhibits anisotropy in both tensile strength and ductility and the trend of anisotropy can be opposing for strength and ductility.[47–49] When inclined walls or struts are present in an AM Ti-6Al-4V structure, their properties may differ in the vertical and horizontal orientations. Post-AM sub-transus (e.g., 950°C/1 h) or super-transus (e.g., 1050°C/1 h) heat treatments can mitigate the degree of anisotropy, but it is difficult to eliminate it.
- Pronounced distortion has been observed for laser-powder-deposited large Ti-6Al-4V structures (1.1 m long) after unclamping them in the as-built state due to relief of residual stresses.[11] Residual stresses were measured to be ~300 MPa in simple as-built SLM Ti-6Al-4V samples.[48] In order to avoid significant distortion, large or intricate laser AM Ti-6Al-4V structures need to be heat treated in a properly clamped form inherited from the as-fabricated state, or subjected to a proper stress-relief annealing treatment.

Electron-beam AM Ti-6Al-4V and effects of heat treatments

Compared with laser AM Ti-6Al-4V, SEBM Ti-6Al-4V can readily satisfy the minimum tensile property requirements for mill-annealed Ti-6Al-4V (see Figure 4b), although occasionally, the tensile elongation may fail to reach 10%. As a result, post-AM heat treatments of SEBM Ti-6Al-4V (excluding HIP) have not received much attention. Large SEBM Ti-6Al-4V structures can be used in the as-built state for non-fatigue critical applications, such as a recently developed honeycomb-structured SEBM Ti-6Al-4V oil-gas separation rotor.[50] Additionally, owing to the relatively high SEBM powder bed temperatures (the substrate is often set at ~730°C; substrate temperatures up to 1100°C were used for SEBM of TiAl),[51] post-AM stress relief annealing is usually unnecessary for SEBM Ti-6Al-4V. Anisotropy in tensile strengths or ductility also occurs in SEBM Ti-6Al-4V, but to a lesser degree in general than in laser AM Ti-6Al-4V.[27,38]

HIP pressing of AM Ti-6Al-4V

HIP of AM Ti-6Al-4V is typically carried out at 920°C for 2 h under 100 MPa in argon,[43] which can close or heal internal pores and lack-of-fusion defects to below the resolution limit of x-ray micro-computer tomography (~5 μm[52]). The use of higher-resolution synchrotron x-ray microtomography (1.5 μm[28]) is expected to further clarify the effectiveness of HIP in closing small pores. Columnar grain boundaries remain after HIP at 920°C. However, owing to the nearly pore-free and equilibrium HIP microstructures, the tensile ductility increases to above 10% for laser AM Ti-6Al-4V, while for SEBM-HIP Ti-6Al-4V, tensile elongation can reach more than 16%.[23] A downside is that AM-HIP Ti-6Al-4V could end up with yield strength below the minimum requirement of 828 MPa (Table I) due to the coarse lamellar α/β and grain boundary α developed during HIP.

The classical Hall–Petch relationship approximately applies to AM Ti-6Al-4V in terms of yield strength varying linearly with the inverse square root of α-lath thickness (**Figure 5**). The α-lath thickness corresponding to the minimum yield strength requirement of 828 MPa is about 8.0 μm (Figure 5). This prediction generally agrees with the coarse lamellar α/β structures of AM-HIP Ti-6Al-4V that show yield strengths below 828 MPa.[23] Consequently, other HIP conditions may need to be explored. The microstructure–property connection shown in Figure 5 served as the roadmap for the recent development of STA-grade SLM Ti-6Al-4V (to be discussed subsequently).

Effects of as-built surface conditions

The tensile properties of AM Ti-6Al-4V previously discussed were obtained from either machined (average roughness $R_a \approx 1$ μm) or polished ($R_a \approx 0.1$–0.5 μm) samples.

https://doi.org/10.1557/mrs.2016.215 Published online by Cambridge University Press

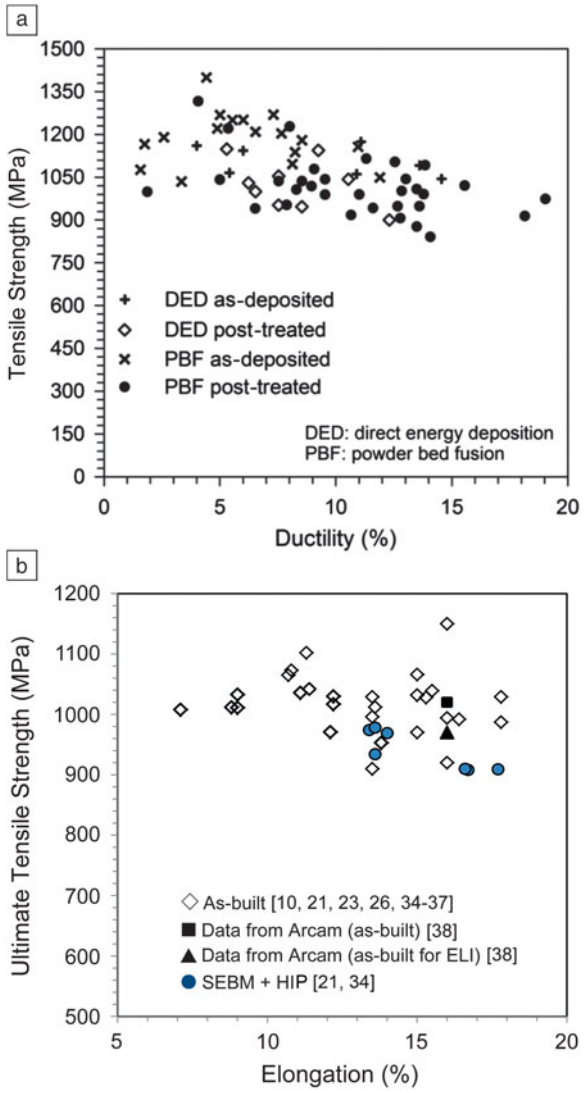

Figure 4. Tensile properties of additively manufactured Ti-6Al-4V with and without post-AM heat treatments: (a) Laser-based AM. Adapted with permission from Reference 37. © 2016 Springer. (b) Selective electron-beam melting (SEBM) results from various studies, including samples that have undergone hot isostatic pressing (HIP). These tensile properties may have been affected by variation in the oxygen content of the powders used; for example, Arcam Ti-6Al-4V powder contains 0.15 wt% oxygen, while Arcam Ti-6Al-4V extra-low interstitial (ELI) powder contains 0.10 wt%.

AM Ti-6Al-4V shows relatively rough surfaces, similar to sand castings ($R_a \approx 12.5$–25 μm).[53] For example, SLM Ti-6Al-4V surfaces typically have $R_a \approx 10$–25 μm, while SEBM Ti-6Al-4V surfaces are usually rougher with R_a up to 40 μm.[54] Consequently, as-built AM Ti-6Al-4V specimens show noticeably lower tensile strengths and ductility, irrespective of the AM process,[19,54–58] as microcracks were found to directly initiate from surface defects.[54,57] Acid etching, surface polishing, and machining have all proved to be effective in improving the surface roughness and therefore the mechanical properties.

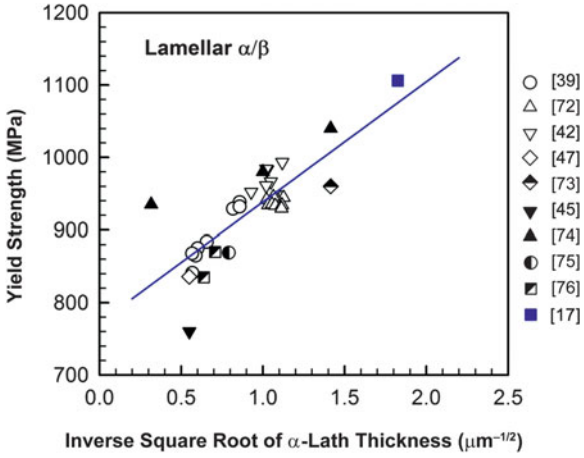

Figure 5. Tensile yield strength versus inverse square root of α-lath thickness for lamellar α/β Ti-6Al-4V. The filled square (blue) corresponds to as-built selective laser melting Ti-6Al-4V with an ultrafine lamellar α/β microstructure (Figure 2b, α-lath thickness: ~300 nm), which attained tensile strength >1200 MPa, yield strength >1100 MPa, and tensile elongation >10%. Adapted with permission from Reference 17. © 2015 Elsevier.

Abrasive fluid machining (AFM) can be another option, although it is more costly. For SEBM Ti-6Al-4V, it appears necessary to remove a ~650-μm-thick surface in order to eliminate the detrimental surface effect.[55] This can be problematic for AM of Ti-6Al-4V components with thin internal sections or struts in lattice structures. In addition, the detrimental influence of the as-built surface conditions on tensile mechanical properties remains after HIP or annealing for both SEBM Ti-6Al-4V and laser powder fusion Ti-6Al-4V.[58] Post-AM surface treatments are thus important to ensure good mechanical properties, regardless of the subsequent heat-treatment process.

As AM technology continues to develop, improved surface conditions, which depend on both the feedstock materials and the AM process, will improve the performance consistency as well as the mechanical properties of the as-built AM Ti-6Al-4V parts. This will be particularly useful for the AM of intricate Ti-6Al-4V components designed for load-bearing applications, due to the difficulty of modifying their internal surfaces, even by acid etching or AFM.

Fatigue properties of AM Ti-6Al-4V

As with other metallic alloys, the fatigue performance of AM Ti-6Al-4V depends on surface conditions, microstructure, and internal defects. No HCF requirements are specified in the ASTM standards for Ti-6Al-4V. **Table II**[29,59–64] lists typical fatigue strengths of non-AM Ti-6Al-4V and the achievable fatigue strengths of AM Ti-6Al-4V in the as-built condition (machined surfaces) by SLM, SEBM, and LMD. Most of the fatigue data reported on AM Ti-6Al-4V in both the as-built and heat-treated conditions have been assessed

https://doi.org/10.1557/mrs.2016.215 Published online by Cambridge University Press

Table II. Fatigue strengths of conventionally manufactured and additively manufactured Ti-6Al-4V tested at $R = 0.1$ (where R is the ratio of minimum to maximum peak stress).

Non-AM Ti-6Al-4V[60,61]		AM Ti-6Al-4V[29,59,62–64]	
Condition	Fatigue strength at 10^7 cycles (MPa)	AM process	Fatigue strength at 10^7 cycles (MPa)*
Cast	200–360	SEBM	Build direction: 390
			Horizontal plane: 450
Cast + HIP	520	SLM, stress relief at 650°C for 4 h	400–510
Mill-annealed	400–680	Laser powder deposition	≥600
Solution-treated and aged (STA)	700	Laser wire (1.2 mm dia., 0.045 wt% O) deposition, 3.5 kW laser power	770–790

*Best fatigue strength data reported in literature for each AM process.

in two recent reviews.[38,65] The following observations are prominent from these assessments[38,65] in conjunction with other fatigue data reported on AM Ti-6Al-4V.[29,66,67]

- Post-AM surface treatments are essential to achieve superior fatigue performance. For example, the fatigue strength of SLM Ti-6Al-4V specimens (Ra ≈ 13 μm) was 210 MPa, compared to 500 MPa for polished SLM Ti-6Al-4V specimens (Ra ≈ 0.5 μm).[63] In addition, shot peening, which entails impacting the surface with round steel particles, has also proved to be effective in improving the fatigue strengths of AM Ti-6Al-4V due to the introduction of a compressive residual stress layer.[68]
- The fatigue strength data of AM Ti-6Al-4V scatter broadly. On the one hand, research has shown that AM Ti-6Al-4V, irrespective of the AM process, can achieve fatigue strengths that are comparable to, or even better than, those of the mill-annealed Ti-6Al-4V (Table II). On the other hand, AM Ti-6Al-4V can be inferior to as-cast Ti-6Al-4V.
- Anisotropic fatigue performance is observed in AM Ti-6Al-4V (Table II) due to the columnar prior-β grain structures, nonuniform distribution of pores and lack-of-fusion defects, and other microstructural features.[29,38]
- HIP can improve the fatigue strength and HCF performance consistency of AM Ti-6Al-4V because of much reduced internal porosity and the elimination of other defects. In general,[38,65] AM-HIP Ti-6Al-4V samples with machined surfaces can show HCF performance (≥550 MPa at 10^7 cycles[58]) fully comparable to, or better than, mill-annealed Ti-6Al-4V. In addition, AM-HIP Ti-6Al-4V exhibits a much smaller degree of anisotropy in fatigue strength than the conventionally heat-treated AM Ti6Al-4V,[38,69] indicating that internal porosity and defects are largely responsible for fatigue anisotropy.
- Appropriate post-AM heat treatments can improve the fatigue strength of AM Ti-6Al-4V. However, since pressureless heat treatments are ineffective to shrink or close pores, HIP is necessary to ensure consistent HCF performance. A potential risk, although not demonstrated yet, is that lack-of-fusion defects and gas pores healed or shrunk by HIP may reopen after a certain number of loading and unloading cycles. A related study has shown that HIP-shrunk pores in SEBM Ti-6Al-4V can grow and reappear during subsequent β annealing due to the high internal argon gas pressure.[70] The argon gas arises from that entrapped in the GA powder as SEBM operates in high vacuum. Again, this shows the necessity of using pore-free powder feedstock for AM of critical parts. SLM Ti-6Al-4V may exhibit a similar or even worse scenario as argon is used as the protective gas during SLM. Wrought Ti-6Al-4V products do not normally have this latent risk.

AM of STA-grade Ti-6Al-4V

Ti-6Al-4V in the STA condition offers the highest strength of the alloy Ti-6Al-4V while still possessing reasonable ductility (Table I). Therefore, it has been used for a variety of applications. The bimodal microstructure of the STA Ti-6Al-4V (globular α + fine lamellar α/β) is, however, not easily achievable by current AM processes.[71]

A recent development has shown that STA-grade tensile mechanical properties are achievable by AM without having to produce a bimodal microstructure.[17] In this new development, the as-built SLM Ti-6Al-4V attained tensile strength >1200 MPa, yield strength >1100 MPa, and tensile elongation >10% (the filled square shown in Figure 5).[17] This was realized by taking advantage of the pronounced formation of martensite in SLM Ti-6Al-4V and allowing the martensite to *in situ* decompose into ultrafine lamellar α/β (Figure 2b, α-lath thickness: ~300 nm) during AM.[17] As shown in Figure 5,[17,39,42,45,47,72–76] ultrafine α laths correspond to high yield strengths. The resulting ultrafine lamellar α-β structure also exhibited good fatigue strength (400 MPa) in the as-built state,[77] although it is still lower than that of the STA Ti-6Al-4V (700 MPa, Table II).

Research is under way to apply this martensite-decomposition-based approach to the AM of Ti-6Al-4V parts with different section thicknesses. Factors that affect the formation and decomposition of martensite in both SLM and SEBM Ti-6Al-4V have received increasing attention for improved microstructural control during AM.[78,79] In addition, unlike martensitic transformation by which martensite laths always form in the parent β grains without changing the parent grain structure, massive transformation in AM Ti-6Al-4V leads to entirely new massive α_m grains (see Figure 2d).[24] This offers a new strategy to transform the columnar β grains in AM Ti-6Al-4V into equiaxed α_m grains. Research has shown that, similar to martensite, α_m can also decompose into ultrafine α/β structures in AM Ti-6Al-4V.[24] The $\beta \rightarrow \alpha_m$ transformation thus offers a different pathway to microstructural and alloy designs for AM. Further microstructural innovations have been

https://doi.org/10.1557/mrs.2016.215 Published online by Cambridge University Press

demonstrated on other AM titanium alloys by taking advantage of the self-aging process during AM (e.g., the realization of 50–250 nm Y_2O_3 precipitates in a SEBM titanium alloy Ti-6Al-2.7Sn-4Zr-0.4Mo-0.45Si-0.1Y).[80]

Concluding remarks

Extensive research performed during the last decade on AM of Ti-6Al-4V alloy has been instrumental in demonstrating the attributes and potential of metal AM technology for industrial applications. AM Ti-6Al-4V in the as-built state (with machined or polished surfaces) can be made to be fully comparable to, or even better than, wrought-grade (mill-annealed) Ti-6Al-4V in terms of both tensile and fatigue performance. However, the mechanical properties can show a large degree of scatter, especially the fatigue strength data, and are often anisotropic. AM build orientation affects both the degree of scatter and the degree of anisotropy.

Pressureless normal post-AM heat treatments in general are not needed for SEBM Ti-6Al-4V, but they are necessary for laser AM Ti-6Al-4V for improved ductility and reduced anisotropy in mechanical properties. Porosity and lack-of-fusion defects remain a major concern, which not only downgrades mechanical performance, but also entails inconsistent and anisotropic responses. Current AM practice with GA Ti-6Al-4V powder can achieve about 99.9% relative density. However, even with 0.1 vol% porosity, the number of damaging pores can still be significant, particularly for fatigue-critical applications. It is desirable to use pore-free powder feedstock providing that neither the availability nor the affordability is an issue.

HIP is a necessary backup to heal or shrink both the internal porosity and lack-of-fusion defects in AM Ti-6Al-4V parts, but there is a potential risk that HIP-shrunk pores may reappear under certain circumstances. The as-built surface conditions exert a noticeable influence on both the tensile and fatigue performance, and the detrimental influence remains after HIP or annealing treatments. Appropriate post-AM surface treatments are necessary for AM Ti-6Al-4V components. Innovative microstructural designs, including design of the pathways to their realization within the specification of Ti-6Al-4V, will continue to hold the key to the development of STA-grade AM Ti-6Al-4V in the as-built state. Further improvements in current AM processes including the feedstock quality and forms that can lead to the fabrication of pore-free AM Ti-6Al-4V can be another major milestone development for the future of metal AM.

Acknowledgments

The authors thank the Australian Research Council (ARC) and National Natural Science Foundation of China (NSFC) for their financial support through ARC DP150104719, ARC LP140100607, and NSFC No. 51528401. They also thank S.L. Lu for useful discussions.

References

1. J.F. Isaza, C. Aumund-Kopp, *Addit. Manuf.* **3**, 41 (2014).
2. K. Ek, "Additive Manufactured Metals," Master of Science thesis, KTH Royal Institute of Technology (2014).
3. M. Qian, *Int. J. Powder Metall.* **46** (5), 29 (2010).
4. J.E. Barnes, W. Peter, C.A. Blue, *Mater. Sci. Forum* **618–619**, 165 (2009).
5. S. Tirelli, E. Chiappini, M. Strano, M. Monno, Q. Semeraro, *Key Eng. Mater.* **651–653**, 1204 (2015).
6. Carpenter Technical Datasheet Titanium Alloy Ti 6Al-4V, http://cartech.ides.com/datasheet.aspx?i=101&E=269 (accessed May 18, 2016).
7. G. Welsch, R. Boyer, E.W. Collings, *Materials Properties Handbook: Titanium Alloys* (ASM International, Materials Park, OH, 1994), p. 517.
8. G.J. Marshall, W.J. Young II, S.M. Thompson, N. Shamsaei, S.R. Daniewicz, S. Shao, *JOM* **68**, 778 (2016).
9. J.E. Craig, T. Wakeman, R. Grylls, J. Bullen, in *Sensors, Sampling, and Simulation for Process Control*, B.G. Thomas, J.A. Yurko, L. Zhang, Eds. (Wiley-TMS, Hoboken, NJ, 2011), pp. 103–110.
10. H.P. Tang, M. Qian, N. Liu, X.Z. Zhang, G.Y. Yang, *JOM* **67**, 555 (2015).
11. C. Qiu, G.A. Ravi, C. Dance, A. Ranson, S. Dilworth, M.M. Attallah, *J. Alloys Compd.* **629**, 351 (2015).
12. E. Brandl, F. Palm, V. Michailov, B. Viehweger, C. Leyens, *Mater. Des.* **32**, 4665 (2011).
13. M. Yan, M.S. Dargusch, T. Ebel, M. Qian, *Acta Mater.* **68**, 196 (2014).
14. R. Dabrowski, *Arch. Metall. Mater.* **56**, 703 (2011).
15. J. Sieniawski, W. Ziaja, K. Kubiak, M. Motyka, in *Titanium Alloys—Advances in Properties Control*, J. Sieniawski, W. Ziaja, Eds. (InTech, Rijeka, Croatia, 2013).
16. T. Ahmed, H.J. Rack, *Mater. Sci. Eng. A* **243**, 206 (1998).
17. W. Xu, M. Brandt, S. Sun, J. Elambasseril, Q. Liu, K. Latham, K. Xia, M. Qian, *Acta Mater.* **85**, 74 (2015).
18. M.N. Ahsan, A.J. Pinkerton, R.J. Moat, J. Shackleton, *Mater. Sci. Eng. A* **528**, 7648 (2011).
19. C. de Formanoir, S. Michotte, O. Rigo, L. Germain, S. Godet, *Mater. Sci. Eng. A* **652**, 105 (2016).
20. P.A. Kobryn, S.L. Semiatin, *J. Mater. Process. Technol.* **135**, 330 (2003).
21. Q. Yuanhong, T. Hua, L. Jing, H. Weidong, *Rare Met. Mater. Eng.* **43**, 2162 (2014).
22. F. Martina, P.A. Colegrove, S.W. Williams, J. Meyer, *Metall. Mater. Trans. A* **46**, 6103 (2015).
23. S.L. Lu, H.P. Tang, Y.P. Ning, N. Liu, D.H. St. John, M. Qian, *Metall. Mater. Trans. A* **46**, 3824 (2015).
24. S.L. Lu, M. Qian, H.P. Tang, M. Yan, J. Wang, D.H. St. John, *Acta Mater.* **104**, 303 (2016).
25. T.B. Massalski, *Metall. Mater. Trans. A* **33**, 2277 (2002).
26. N. Sridharan, A. Chaudhary, P. Nandwana, S.S. Babu, *JOM* **68**, 772 (2016).
27. H. Galarraga, D.A. Lados, R.R. Dehoff, M.M. Kirka, P. Nandwana, *Addit. Manuf.* **10**, 47 (2016).
28. R. Cunningham, S.P. Narra, T. Ozturk, J. Beuth, A.D. Rollett, *JOM* **68**, 765 (2016).
29. S. Tammas-Williams, H. Zhao, F. Léonard, F. Derguti, I. Todd, *Mater. Charact.* **102**, 47 (2015).
30. M. Svensson, U. Ackelid, *Proc. Mater. Process. Med. Devices Conf. 2009*, J. Gilbert, Ed. (Minneapolis, MN, 2010), pp. 189–194.
31. B. Vandenbroucke, J.P. Kruth, *Rapid Prototyp. J.* **13**, 196 (2007).
32. T. Becker, M. van Rooyen, D. Dimitrov, *S. Afr. J. Ind. Eng.* **26**, 93 (2015).
33. J.J.Z. Li, W.L. Johnson, W.-K. Rhim, *Appl. Phys. Lett.* **89**, 111913 (2006).
34. S.A. Khairallah, A.T. Anderson, A. Rubenchik, W.E. King, *Acta Mater.* **108**, 36 (2016).
35. T. Saito, T. Furuta, US Patent 5,409,518 (1995).
36. Timetal Datasheet on Ti-6Al-4V, http://www.timet.com/datasheets-and-literature (accessed May 20, 2016).
37. A.M. Beese, B.E. Carroll, *JOM* **68**, 724 (2016).
38. L. Bian, S.M. Thompson, N. Shamsaei, *JOM* **67**, 629 (2015).
39. S.S. Al-Bermani, M.L. Blackmore, W. Zhang, I. Todd, *Metall. Mater. Trans. A* **41**, 3422 (2010).
40. L.E. Murr, E.V. Esquivel, S.A. Quinones, S.M. Gaytan, M.I. Lopez, *Mater. Charact.* **60**, 96 (2009).
41. H. Gong, K. Rafi, H. Gu, G.D. Janaki Ram, T. Starr, B. Stucker, *Mater. Des.* **86**, 545 (2015).
42. N. Hrabe, T. Quinn, *Mater. Sci. Eng. A* **573**, 271 (2013).
43. Arcam AB Ti6A14V Titanium Alloy, http://www.arcam.com/wp-content/uploads/Arcam-Ti6Al4V-Titanium-Alloy.pdf (accessed May 20, 2016).
44. Q. Huang, X. Liu, X. Yang, R. Zhang, Z. Shen, Q. Feng, *Front. Mater. Sci.* **9**, 373 (2015).
45. B. Vrancken, L. Thijs, J.P. Kruth, J. Van Humbeeck, *J. Alloys Compd.* **541**, 177 (2012).
46. M. Thöne, S. Leuders, A. Riemer, T. Tröster, H.A. Richard, *Proc. 23rd Solid Freeform Fabr. Symp. (SFF)* (The University of Texas at Austin, Austin, TX, 2012), pp. 492–498, http://sffsymposium.engr.utexas.edu/Manuscripts/2012/2012-38-Thoene.pdf (accessed May 20, 2016).

https://doi.org/10.1557/mrs.2016.215 Published online by Cambridge University Press

47. T. Vilaro, C. Colin, J.D. Bartout, *Metall. Mater. Trans. A* **42**, 3190 (2011).
48. M. Simonelli, Y.Y. Tse, C. Tuck, *Mater. Sci. Eng. A* **616**, 1 (2014).
49. X. Zhao, S. Li, M. Zhang, Y. Liu, T.B. Sercombe, S. Wang, Y. Hao, R. Yang, L.E. Murr, *Mater. Des.* **95**, 21 (2016).
50. H.P. Tang, Q.B. Wang, G.Y. Yang, J. Gu, N. Liu, L. Jia, M. Qian, *JOM* **68**, 799 (2016).
51. H.P. Tang, G.Y. Yang, W.P. Jia, W.W. He, S.L. Lu, M. Qian, *Mater. Sci. Eng. A* **636**, 103 (2015).
52. S. Tammas-Williams, P.J. Withers, I. Todd, P.B. Prangnell, *Metall. Mater. Trans. A* **47**, 1939 (2016).
53. Surface roughness produced by different manufacturing process, http://www.meadinfo.org/2009/06/surface-finish-roughness-ra.html (accessed August 15, 2016).
54. Y.Y. Sun, S. Gulizia, C.H. Oh, D. Fraser, M. Leary, Y.F. Yang, M. Qian, *JOM* **68**, 791 (2016).
55. S. Palanivel, A.K. Dutt, E.J. Faierson, R.S. Mishra, *Mater. Sci. Eng. A* **654**, 39 (2016).
56. G. Kasperovich, J. Hausmann, *J. Mater. Process. Technol.* **220**, 202 (2015).
57. J. Alcisto, A. Enriquez, H. Garcia, S. Hinkson, T. Steelman, E. Silverman, P. Valdovino, H. Gigerenzer, J. Foyos, J. Ogren, J. Dorey, *J. Mater. Eng. Perform.* **20**, 203 (2011).
58. D. Greitemeier, F. Palm, F. Syassen, T. Melz, *Int. J. Fatigue*, published online May 3, 2016, http://dx.doi.org/10.1016/j.ijfatigue.2016.05.001.
59. R. Grylls, Ed., "LENS Process White Paper: Fatigue Testing of LENS Ti-6-4," http://www.optomec.com/wp-content/uploads/2014/04/LENS_fatique-testing_whitepaper.pdf (accessed May 25, 2016).
60. M.J. Donachie, *Titanium: A Technical Guide*, 2nd ed. (ASM International, Materials Park, OH, 2000).
61. Titanium Ti-6Al-4V (Grade 5), STA, http://asm.matweb.com/search/SpecificMaterial.asp?bassnum=MTP642 (accessed August 15, 2016).
62. H.K. Rafi, T.L. Starr, B.E. Stucker, *Int. J. Adv. Manuf. Technol.* **69**, 1299 (2013).
63. E. Wycisk, A. Solbach, S. Siddique, D. Herzog, F. Walther, *Phys. Procedia* **56**, 371 (2014).
64. B. Baufeld, E. Brandl, O. Van der Biest, *J. Mater. Process. Technol.* **211**, 1146 (2011).
65. P. Li, D.H. Warner, A. Fatemi, N. Phan, *Int. J. Fatigue* **85**, 130 (2016).
66. D. Greitemeier, F. Palm, F. Syassen, T. Melz, *Int. J. Fatigue* (forthcoming).
67. P. Åkerfeldt, R. Pederson, M.L. Antti, *Int. J. Fatigue* **87**, 245 (2016).
68. E.R. Wycisk, C.L. Emmelmann, S. Siddique, F. Walther, *Adv. Mater. Res.* **816**, 134 (2013).
69. M.-W. Wu, P.-H. Lai, *Mater. Sci. Eng. A* **658**, 429 (2016).
70. S. Tammas-Williams, P.J. Withers, I. Todd, P.B. Prangnell, *Scr. Mater.* **122**, 72 (2016).
71. M. Simonelli, Y.Y. Tse, C. Tuck, *J. Mater. Res.* **29**, 2028 (2014).
72. N. Hrabe, T. Quinn, *Mater. Sci. Eng. A* **573**, 264 (2013).
73. S. Zherebtsov, G. Salishchev, R. Galeyev, K. Maekawa, *Mater. Trans.* **46**, 2020 (2005).
74. L. Wagner, J.K. Bigoney, "Fatigue of Titanium Alloys," in *Titanium and Titanium Alloys: Fundamentals and Applications*, C. Leyens, M. Peters, Eds. (Wiley, Weinheim, 2003), p. 153.
75. H.K. Rafi, N.V. Karthik, H.J. Gong, T.L. Starr, B.E. Stucker, *J. Mater. Eng. Perform.* **22**, 3872 (2013).
76. L. Facchini, E. Magalini, P. Robotti, A. Molinari, S. Hoges, K. Wissenbach, *Rapid Prototyp. J.* **16**, 450 (2010).
77. W. Xu, S. Sun, J. Elambasseril, Q. Liu, M. Brandt, M. Qian, *JOM* **67**, 668 (2015).
78. J. Yang, H. Yu, J. Yin, M. Gao, Z. Wang, X. Zeng, *Mater. Des.* **108**, 308 (2016).
79. X. Tan, Y. Kok, W.Q. Toh, Y.J. Tan, M. Descoins, D. Mangelinck, S.B. Tor, K.F. Leong, C.K. Chua, *Sci. Rep.* **6**, 26039 (2016).
80. S.-L. Lu, H.-P. Tang, M. Qian, L.-Y. Zeng, D.H. St. John, *J. Cent. South Univ.* **22**, 2857 (2015). □

https://doi.org/10.1557/mrs.2016.215 Published online by Cambridge University Press

Become an MRS Congressional Science and Engineering Fellow!

Help **improve the interface** between science and legislative decision making.

Advocate for policies that will facilitate the discoveries of the future.

Play a crucial role as you **educate the public** about the benefits of science.

Decisions made by Congress, regulatory agencies and local government have profound effects on the way in which science is conducted. By keeping decision makers well informed on the current affairs of the scientific community, MRS Congressional Science and Engineering Fellows ensure the right choices are being made. Now's your time to make a difference!

The Materials Research Society offers materials scientists two exciting opportunities to participate in, and contribute to, the federal policymaking process, while learning firsthand about the intersection of science and policy.

During your year as a Fellow you will:

- contribute widely to the effective use of materials science knowledge in government
- broaden awareness about the value of scientist- and engineer-government interaction among society members and within government
- have significant freedom to follow specific topics and issues that interest you

The MRS Congressional Science and Engineering Fellowship Program is an invaluable experience, but don't just take our word for it. Our past Congressional Fellows explain it best!

"Academia taught me how to think, but the MRS Congressional Fellowship taught me how to get things done. Never have I had such leverage, such opportunities to comingle with dignitaries, to structure agreements and broker deals, as I did in that year. I learned how to navigate past armies of secretaries shielding a VIP, enlist military support for a project, take a rough idea and make it law, to fashion an event into a sound bite and then watch it propagate across the news. I learned to take data and present it in such a way that it gravitated, almost of its own accord, all the way up to the Vice President of the United States. These are skills anyone, who is going anywhere, can use."

Merrilea Mayo Founder, Mayo Enterprises, LLC.
MRS Congressional Fellow 1998–1999
Office of Senator Lieberman

"At the end of the fellowship year I found that I was enjoying 'doing' science policy more than just teaching about it, and I ended up staying on in Rep. Honda's office as a member of the staff where I have remained for over a decade. I would not have had that opportunity without the Congressional Fellowship. I encourage anyone who wonders about how federal policies are developed or wants to have a greater role in that process to apply to be a Congressional Fellow."

Eric Werwa Legislative Director, Congressman Mike Honda
MRS Congressional Fellow 2001–2002
Office of Congressman Mike Honda

MRS® To learn more about the MRS Congressional Science and Engineering Fellowship Program and how you can apply, visit **www.mrs.org/congressional-fellows**.

Applications for the MRS-OSA Fellowship must be postmarked or emailed by 11:59 p.m. (ET), Friday, January 6, 2017.

Applications for the MRS-TMS Fellowship must be submitted through the MRS Awards Nomination Submission Portal (https://awards.mrs.org) and must be received by 11:59 p.m. (ET), Friday, January 6, 2017.

https://doi.org/10.1557/mrs.2016.215 Published online by Cambridge University Press